Determining the optical properties of turbid media by using the adding–doubling method

Scott A. Prahl, Martin J. C. van Gemert, and Ashley J. Welch

A method is described for finding the optical properties (scattering, absorption, and scattering anisotropy) of a slab of turbid material by using total reflection, unscattered transmission, and total transmission measurements. This method is applicable to homogeneous turbid slabs with any optical thickness, albedo, or phase function. The slab may have a different index of refraction from its surroundings and may or may not be bounded by glass. The optical properties are obtained by iterating an adding–doubling solution of the radiative transport equation until the calculated values of the reflection and transmission match the measured ones. Exhaustive numerical tests show that the intrinsic error in the method is $< 3\%$ when four quadrature points are used.

1. Introduction

This paper introduces a practical way to determine the optical properties of scattering and absorbing materials. These properties are obtained by repeatedly solving the radiative transport equation until the solution matches the measured reflection and transmission values. The advantages over existing methods are increased accuracy and flexibility in modeling turbid samples with intermediate albedos, mismatched boundary conditions, and anisotropic scattering. The primary disadvantage is that this method is entirely numerical. For brevity this method is called inverse adding–doubling (IAD): inverse implies a reversal of the usual process of calculating reflection and transmission from optical properties, and adding–doubling indicates the method used to solve the radiative transport equation. The IAD algorithm and theory are described in this paper; an experimental implementation is presented in the companion paper.[1]

The optical properties of biological tissue are important for photodynamic therapy and diagnostic techniques.[2] Typically optical properties are obtained by using solutions of the radiative transport equation that express the optical properties in terms of readily measurable quantities.[3] These solutions are either exact or approximate and correspond to the direct or indirect methods described by Wilson *et al.*[4] Direct methods place stringent constraints on the sample to match the assumptions made for the exact solution. For example, the direct method used by Flock *et al.*[5] required thin samples in which multiple scattering could be ignored. Indirect methods relax the sample constraints but require approximations that are often invalid for tissue samples (e.g., nearly isotropic scattering or no internal reflection at the boundaries). The theory used in indirect methods usually falls into one of three categories: Beer's law, Kubelka–Munk, or the diffusion approximation.

Beer's law neglects scattering and is inappropriate for thick scattering materials. The Kubelka–Munk method and variants[6–12] are still used[13,14] but are limited in their accuracy.[11,15] Methods based on the diffusion approximation or a similar approximation (e.g., uniform radiances over the forward and backward hemispheres) tend to be more accurate than the Kubelka–Munk method.[16,17] Techniques using the diffusion approximation include pulsed photothermal radiometry,[18] time-resolved spectroscopy,[19] radial reflectance spectroscopy,[20] weak localization,[21] and an iterative technique that uses reflection and transmission measurements.[22] These methods remain popular because they are easy to use, place relatively minor constraints on the type of sample, and are amenable to analytic manipulation. However, the diffusion approximation assumes that the internal

S. A. Prahl is with the Department of Electrical Engineering and Applied Physics, Oregon Graduate Institute, Beaverton, Oregon 97006. M. J. C. van Gemert is with the Laser Center, Academic Medical Center, Amsterdam, The Netherlands. A. J. Welch is with Biomedical Engineering, University of Texas at Austin, Austin, Texas 78712.

Received 8 January 1992
0003-6935/93/040559-10$05.00/0.

radiance is nearly isotropic, and consequently it is inaccurate when scattering is comparable with absorption.[23]

The adding–doubling method is a general, numerical solution of the radiative transport equation.[24] The adding–doubling method[25] was chosen because it is sufficiently fast that iterated solutions are possible on current microcomputers and sufficiently flexible that anisotropic scattering and internal reflection at the boundaries may be included. Other accurate solutions of the radiative transport equation such as Chandrasekhar's X and Y functions,[26] discrete ordinates,[27] Monte Carlo models,[28–30] invariant embedding,[31] or successive orders[24] are too slow or insufficiently flexible to incorporate the necessary boundary conditions needed for turbid materials with mismatched boundaries.

The IAD method consists of the following steps: (1) Guess a set of optical properties. (2) Calculate the reflection and transmission by using the adding–doubling method. (3) Compare the calculated values with the measured reflection and transmissions. (4) Repeat until a match is made. The set of optical properties that generates reflection and transmission values matching the measured values is taken as the optical properties of the sample. The results obtained with the IAD method are accurate for all optical properties and can be made arbitrarily precise at the cost of increased computation time. Furthermore, by avoiding an analytical solution, it is possible to incorporate the necessary corrections for measurements made directly with integrating spheres[32] (see Section 3.F). Such corrections are usually quite awkward to implement because the magnitude of the correction depends on the optical properties of the sample measured.

2. Adding–Doubling Method

A. Definitions

The optical properties of a turbid medium are characterized by the absorption coefficient μ_a, the scattering coefficient μ_s, and the single-scattering phase function $p(\theta)$. The reciprocal of the absorption (scattering) coefficient is the average distance a photon will travel before being absorbed (scattered) by the medium. Two dimensionless quantities that characterize light propagation in a turbid medium are the albedo a and the optical thickness τ. These are defined as

$$a = \frac{\mu_s}{\mu_s + \mu_a}, \qquad \tau = d(\mu_s + \mu_a),$$

where d is the physical thickness of the slab.

The single-scattering phase function $p(\theta)$ describes the amount of light scattered at an angle θ from the incoming direction. The phase function is often expressed in terms of the cosine of this scattering angle $\nu = \cos\theta$. The phase function is normalized so that its integral over all directions is unity:

$$\int_{4\pi} p(\nu)\mathrm{d}\omega = 2\pi \int_{-1}^{1} p(\nu)\mathrm{d}\nu = 1,$$

where $d\omega$ is a differential solid angle. The functional form of the phase function in tissue is usually not known. However, research by Jacques *et al.*[33] and Yoon *et al.*[34] have shown that a Henyey–Greenstein function approximates single-particle light scattering in human dermis and aorta at 633 nm. Consequently this phase function is used in all calculations in this paper:

$$p(\nu) = \frac{1}{4\pi}\frac{1 - g^2}{(1 + g^2 - 2g\nu)^{3/2}}.$$

The Henyey–Greenstein phase function depends on only the anisotropy coefficient g, defined as

$$g = \int_{4\pi} p(\nu)\nu\mathrm{d}\omega = 2\pi \int_{-1}^{1} p(\nu)\nu\mathrm{d}\nu.$$

Consequently g is the average cosine of the scattering angle. When $g = 0$, scattering is equally probable in all directions. Typical values for tissues in the red region of the spectrum are $g \approx 0.8$,[2] which is moderately forwardly directed.

Reflection and transmission are relative to the normal irradiance on the sample surface and vary between zero and one. The total reflection R_T is all light specularly reflected and backscattered by the sample. The total transmission T_T is all the light that passes through the sample and includes any light traveling through the sample without being scattered. This unscattered light is denoted T_C, because for collimated irradiance on a sample the light passing directly through the sample is often called the collimated transmission. For a nonabsorbing sample $R_T + T_T = 1$.

B. Theory

The doubling method was introduced by van de Hulst for solving the radiative transport equation in a slab geometry.[35] The advantages of the adding–doubling method are that only integrations over angle are required, physical interpretation of results can be made at each step, the method is equivalent for isotropic and anisotropic scattering, and results are obtained for all angles of incidence used in the integration.[36] The disadvantages are that (a) it is slow and awkward for calculating internal fluences, (b) it is suited to a layered geometry with uniform irradiation, and (c) it is necessary that each layer have homogeneous optical properties. For determining optical properties using only reflection and transmission, internal fluences are not needed, so disadvantage (a) is not a problem. Disadvantages (b) and (c) place restrictions on the sample geometry—the samples must be uniformly illuminated, homogeneous slabs. The adding–doubling method is well suited to

iterative problems because it provides accurate total reflection and transmission calculations with relatively few quadrature points. The method is fast for small numbers of quadrature points, and consequently iteration is practical.

In all calculations that follow the following assumptions are made: the distribution of light is independent of time, samples have homogeneous optical properties, the sample geometry is an infinite plane-parallel slab of finite thickness, the tissue has a uniform index of refraction, internal reflection at boundaries is governed by Fresnel's law, and the light is unpolarized. A nonabsorbing layer with a different index of refraction may be present at the boundaries (glass slide).

The doubling method assumes that the reflection $R(\nu, \nu')$ and transmission $T(\nu, \nu')$ for light incident at an angle ν and exiting at an angle ν' is known for one layer. The reflection and transmission of a slab that is twice as thick is found by juxtaposing two identical slabs and adding the reflection and transmission contributions from each slab.[25] The reflection and transmission for an arbitrary slab are calculated first by finding the reflection and transmission for a thin starting slab with the same optical properties (e.g., by using single scattering) and then by doubling until the desired thickness is reached. The adding method extends the doubling method to dissimilar slabs. Thus slabs with different optical properties can be placed adjacent to one another to simulate layered media or internal reflection caused by index-of-refraction differences.

C. Internal Reflection and Boundary Conditions

Internal reflection at the boundaries (caused by mismatched indices of refraction) was included in the calculation by adding an additional layer for each mismatched boundary. The reflection and transmission of this layer equaled the Fresnel reflection and transmission for unpolarized light incident on a plane boundary between two transparent media with the same indices of refraction. If $r(\nu_i)$ is the unpolarized Fresnel reflection for light incident from a medium with the index of refraction n_1 on a medium with an index of refraction n_2 at an angle from the normal with the cosine equal to ν_i, the reflection and transmission operators for the boundary slab are

$$R_{\text{bndry}}(\nu_i, \nu_j) = \frac{r(\nu_i)}{2\nu_i}\delta_{ij}, \quad T_{\text{bndry}}(\nu_i, \nu_j) = \frac{1 - r(\nu_i)}{2\nu_i}\left(\frac{n_1}{n_0}\right)^2\delta_{ij}, \tag{1}$$

where δ_{ij} is the Kronecker delta function. The square of the ratio of the indices of refraction is due to the n^2 law of radiance,[37] which accounts for the difference in radiances across an index-of-refraction mismatch. The factor of $2\nu_i$ is included for uniformity with van de Hulst's definition of the reflection function.[24] Note finally that the transmission and reflection of the boundary layer were zero and one, respectively, for light that is incident at angles exceeding the critical angle for total internal reflection. Both operators are diagonal because light is specularly reflected and the angle of incidence equals the angle of reflection.

By sandwiching a tissue sample between glass or quartz plates, we can minimize the usual irregularities in the tissue surface, and the Fresnel reflection is a good approximation. To account for a nonabsorbing boundary with a different index of refraction, we must include all the multiple internal reflections.[2] For example, if ν_i is the cosine of the angle of incidence from the turbid slab (index n_s) onto a glass slide (index n_g), the cosine of the angle inside the glass slide (ν_g) is determined by using Snell's law:

$$n_g(1 - \nu_g^2)^{1/2} = n_s(1 - \nu_i^2)^{1/2}, \qquad \nu_i < \nu_c,$$

where ν_c is the cosine of the critical angle for total internal reflection. When $r_i = r(\nu_i)$ is defined as the unpolarized Fresnel reflection coefficient for light passing from the slab into glass and $r_g = r(\nu_g)$ is for light passing from glass to air, the net reflection coefficient that should be used in Eqs. (1) is

$$r(\nu) = \begin{cases} \dfrac{r_1(\nu_i) + r_g(\nu_g) - 2r_1(\nu_i)r_g(\nu_g)}{1 - r_1(\nu_i)r_g(\nu_g)} & \text{if } \nu_i < \nu_c \\ 1 & \text{if } \nu_i \geq \nu_c \end{cases}.$$

This value for $r(\nu)$ accounts for the extra reflections within the glass slide. Finally, since light is refracted at the boundary, we must be sure that the incident and reflected fluxes are identified with the proper angles.

The reflection and transmission functions for the thin starting layers were obtained by the diamond initialization method.[38] The optical thickness for the starting layers was based on the smallest quadrature angle as suggested by Wiscombe.[39] The Henyey–Greenstein phase function was used for all calculations. We avoided phase-function renormalization by always using the $\delta - M$ method, which facilitates accurate calculations with highly anisotropic phase functions.[40]

The adding–doubling method is based on the numerical integration of functions with quadrature:

$$\int_0^1 f(\nu, \nu')\mathrm{d}\nu' = \sum_{k=1}^{N} H_k f(x_k).$$

The quadrature points x_k and weights H_k are chosen so that the integral is approximated exactly for a polynomial of order $2N - 1$ (or possibly $2N - 2$, depending on the quadrature method). Using N quadrature points (Gaussian quadrature) is equivalent to the spherical harmonic method of order P_{N-1},[41] i.e., four quadrature points correspond to the P_3 method. The choice of quadrature methods is described in Section 3.

The total internal reflection caused problems by changing the effective range of integration. Usually adding–doubling integrals range from 0 to 1, since

the angle varies from $\pi/2$ to 0 and therefore the cosine varies from 0 to 1. We used numerical quadrature in calculating the integrations, and the quadrature angles were optimized for this range. If the cosine of the critical angle is denoted by ν_c, then for a boundary layer with total internal reflection the effective range of integration is reduced down to ν_c to 1 (because the rest of the integration range is now 0). To maintain integration accuracy, we separated the integral into two parts, and each is evaluated by quadrature over the specified subrange:

$$\int_0^1 A(\nu, \nu')B(\nu', \nu'')\mathrm{d}\nu' = \int_0^{\nu_c} A(\nu, \nu')B(\nu', \nu'')\mathrm{d}\nu' + \int_{\nu_c}^1 A(\nu, \nu')B(\nu', \nu'')\mathrm{d}\nu'.$$

Here $A(\nu, \nu')$ and $B(\nu, \nu')$ represent reflection or transmission functions, and, if either is identically zero for $\nu < \nu_c$, then the integration range is reduced. The calculations in this paper used Gaussian quadrature[42] for the range from 0 to ν_c, and thereby calculations at both end points were avoided. (In particular the angle $\nu = 0$ is avoided, which may cause division by zero.) Radau quadrature was used for the range from ν_c to 1, because one quadrature angle may be specified.[43] Normal irradiance corresponds to $\nu = 1$, and if this angle is specified, interpolation between quadrature points is not needed to obtain reflection and transmission for normal unscattered irradiance. Interpolation can be a significant source of error. The number of quadrature points are divided evenly between 0 to ν_c and ν_c to 1. Since the quadrature methods work well with even numbers of quadrature points, this dictates that the quadrature points should be chosen in multiples of four. Radau quadrature was used when there was no critical angle.

3. Iteration Process

The iteration process consists of finding optical properties that generate the measured reflection and transmission values. This section begins by showing that a unique solution to the inverse problem exists, and then the simplifications that are necessary when one or more of the experimental measurements is missing are described. Finally three components of the iteration process are given: (1) the function that defines the distance the calculated values are from the measure values, (2) the initial set of optical properties guessed, and (3) the algorithm used to minimize this function.

A. Uniqueness

The iteration method implicitly assumes that a unique combination of the albedo, the optical depth, and the anisotropy is determined by a set of reflection and transmission measurements. Clearly, if a sample is so thick that an accurate unscattered transmission measurement cannot be made, there are more unknowns than observations. Even when all the measurements are available, it is not obvious that a unique set of optical properties (a, τ, g) exists for any set of measurements (R_T, T_T, T_C). For example, increasing the albedo of a sample will increase its total reflection and decrease its total transmission—but so will increasing the optical thickness of the sample. Uniqueness is demonstrated for two cases: fixed unscattered transmission and fixed scattering anisotropy. The former is representative when (R_T, T_T, T_C) are all known; the latter applies when the unscattered transmission measurement is unavailable and a fixed value for the scattering anisotropy must be assumed.

The dependence of the total transmission and total reflection on the anisotropy and albedo is shown in Fig. 1. The bold (a, g) grid was computed with the unscattered transmission fixed at 10% ($T_C = 0.1$), and the boundaries of the sample were matched with its environment. The intersection of the measured total reflection and total transmission grid lines determines a unique albedo and anisotropy.

In Fig. 2 the dependence of the total transmission and the total reflection on the reduced albedo and reduced optical thickness is shown. Scattering in the medium is assumed to be isotropic ($g = 0$), and the index of refraction is 1.4.[44] Again, any nonzero reflection and transmission measurement yields a unique value for the reduced scattering and absorption coefficient. Figure 2 is quite useful for obtaining quick estimates of the optical properties of a sample. For example, if $R_T = 0.4$ and $T_T = 0.2$, then $a \approx 0.96$ and $\tau \approx 7$. If the thickness of the sample is 0.4 mm and the scattering anisotropy is assumed to be ≈ 0.8, using the similarity relations (see below) will fix the optical properties at $(\mu_a, \mu_s, g) \approx (0.7\ \mathrm{mm}^{-1}, 17\ \mathrm{mm}^{-1}, 0.8)$.

C. Simplification

The three measurements usually available are the total reflection, the total transmission, and the unscat-

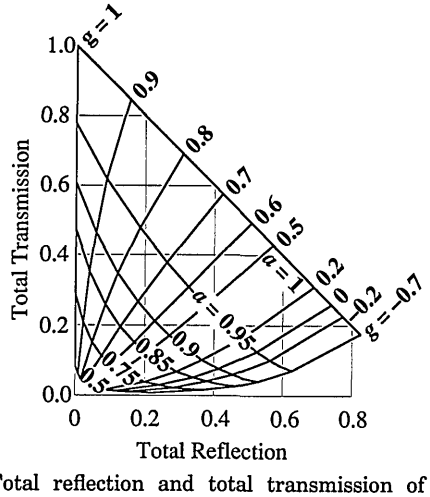

Fig. 1. Total reflection and total transmission of an index-matched slab ($n = 1$) as a function of the albedo a and anisotropy g for a fixed unscattered transmission value of 10%. Each point on the bold (a, g) grid corresponds to a unique (R_T, T_T) pair.

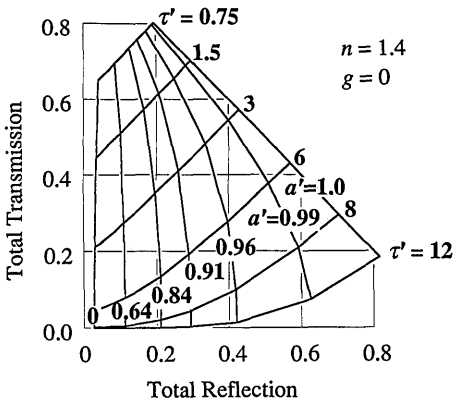

Fig. 2. Total reflection and total transmission of a slab as a function of the reduced albedo a' and reduced optical thickness τ'. Isotropic scattering is assumed as well as an index of refraction mismatch ($n = 1.4$). Each point on the (a', τ') grid corresponds to a unique (R_T, T_T) pair.

tered transmission. It is assumed that the unscattered reflection from each surface is equal to the Fresnel reflection for the unpolarized light that is normally incident on the sample. From the unscattered transmission T_C, we may immediately calculate the optical thickness τ by solving

$$T_C = \frac{(1 - r_{s1})(1 - r_{s2})\exp(-\tau)}{1 - r_{s1}r_{s2}\exp(-2\tau)}, \qquad (2)$$

where r_{s1} and r_{s2} are the primary reflections for light that is normally incident on the front and back surfaces of the slab. If glass slides are present, the specular reflection coefficients r_{s1} and r_{s2} should include multiple internal reflections in the slide (see Subsection 2.C). Once the optical thickness is known, only the albedo and anisotropy remain to be determined. They are varied until the calculated reflection and transmission match the measured values.

When the only measurements available are the total reflection and transmission, as might happen for a thick sample in which an accurate unscattered transmission measurement cannot be made, only two optical parameters can be determined. Typically a value for the scattering anisotropy is assumed, and the albedo and optical thickness are calculated based on this assumed value. The accuracy of say fluence calculations when these values are used (based on similarity) is unknown.

If only one measurement is available, the sample is usually too thick for a transmission measurement to be made. In this case the optical thickness of the sample is assumed to be infinite, and again a fixed value for the scattering anisotropy is chosen. The reduced albedo can now be calculated. This is a simple one-parameter minimization problem, and convergence is robust and rapid.

C. Metric

When the reflection and transmission for a particular set of optical properties are calculated, a definition of how far these values are from those measured is needed. Several metrics were tried, but one based on a sum of relative errors worked best:

$$M(a, \tau, g) = \frac{|R_{\text{calc}} - R_{\text{meas}}|}{R_{\text{meas}} + 10^{-6}} + \frac{|T_{\text{calc}} - T_{\text{meas}}|}{T_{\text{meas}} + 10^{-6}}.$$

Here R_{meas} and T_{meas} are the measured reflection and transmission for scattered light. The factor of 10^{-6} is included to prevent division by zero when the reflection or transmission is zero. Note that the measurement errors for reflection and transmission are assumed to be equal for this metric. If this is not true, suitable modifications are necessary.

D. Inverse Method

The iteration method uses an N-dimensional minimization algorithm based on the downhill simplex method of Nelder and Mead.[45] One implementation of this method (AMOEBA) varies the parameters from $-\infty$ to ∞.[42] Since the anisotropy, albedo, and optical depth have fixed ranges, they are transformed into a computation space. For example, the transformation function for the albedo is

$$a_{\text{comp}} = \frac{2a - 1}{a(1 - a)}.$$

Thus, as a_{comp} varies from $-\infty$ to ∞, the albedo a varies from 0 to 1. The transformation for the anisotropy g (which varies from -1 to 1) is

$$g_{\text{comp}} = \frac{g}{1 + |g|}.$$

The transformation for the optical thickness τ (which varies from 0 to ∞) is

$$b_{\text{comp}} = \ln(\tau).$$

We can easily invert these relations to obtain relations for the optical properties in terms of the computation values. We made all calculations by using the real values: the transformed values were used only by the simplex method for choosing the next iteration point. Typical convergence was in 20–30 iterations.

E. Initial Values

The starting set of optical properties affects both the rapidity of convergence and the convergence to the correct values. Clearly, with a better first guess, fewer subsequent iterations are needed. Poor guesses have the added disadvantage that the minimization algorithm may converge to a relative rather than the global minimum. Since the global minimum corresponds to the unique solution described above, local minima must be guarded against. Fortunately they are easily detected by examining the magnitude of the minimum. If the magnitude exceeds a small tolerance (typically 10^{-3}), the minimum is a local one and the iteration process must be restarted with a better initial guess. If necessary,

$$\frac{P_r}{P} = \frac{\gamma_1[R_c(1-\gamma_2 R_d)+\gamma_3 R_{cd}](1-\gamma_4 R_d)+\gamma_1\gamma_3\gamma_4 T_d(T_{cd}+\gamma_5 T_C)}{(1-\gamma_4 R_d)(1-\gamma_6 R_d)-\gamma_4\gamma_6 T_d^2},$$

one or two restarts suffice to reach the global minimum.

Generating an initial set of approximately correct optical properties for any reflection and transmission combination is difficult. We can use the similarity relations[46] to facilitate picking starting values by relating (a, τ, g) to the reduced optical properties $(a', \tau', g' = 0)$:

$$a' = \frac{a(1-g)}{1-ag}, \qquad \tau' = (1-ag)\tau. \tag{3}$$

The inverse relations are

$$a = \frac{a'}{1-g+a'g}, \qquad \tau = \tau' + \frac{a'\tau' g}{1-g}. \tag{4}$$

Now only two parameters need to be found (a', τ') for a combination (R_T, T_T). For example, originally the Kubelka–Munk relations were used to obtain these values for initial guesses.[47] Unfortunately these values were often worse than using just a fixed guess $(a', \tau', g) = (0.5, 1, 0.2)$ to begin all iterations. A good starting set of starting values is based on a crude fit of the reflection and transmission values of Fig. 2. The formula for the reduced albedo is

$$a' = \begin{cases} 1 - \left(\dfrac{1-4R_d-T_T}{1-T_T}\right)^2 & \text{if } \dfrac{R_d}{1-T_T} < 0.1 \\ 1 - \dfrac{4}{9}\left(\dfrac{1-R_d-T_T}{1-T_T}\right)^2 & \text{if } \dfrac{R_d}{1-T_T} \geq 0.1. \end{cases}$$

The formula for the reduced optical thickness is

$$\tau' = \begin{cases} \dfrac{-\ln T_T \ln(0.05)}{\ln R_T} & \text{if } R_d \leq 0.1 \\ 2^{1+5(R_d+T_T)} & \text{if } R_d > 0.1. \end{cases}$$

Once we obtain τ by using Eq. (3), and a' and τ' have been calculated as above, Eqs. (1) and (2) can be used to generate a single set of starting values (a, τ, g). This is the only time the similarity relations are used in the IAD method.

F. Integrating-Sphere Correction

Total transmission and reflection are usually measured with integrating spheres. Interaction between the sample and spheres makes the detected signal no longer proportional to the sample reflection or transmission.[32] For example, when a double-integrating-sphere arrangement is used, the power on the wall of the reflectance sphere P_r normalized to the incident power P is[32]

where the γ_i values depend on only the geometry and reflectivity of the integrating spheres, and various R and T values correspond to different types of reflection and transmission by the sample. A similar formula holds for the normalized power on the transmission sphere wall. Once the integrating spheres have been characterized (i.e., the γ_i values are known), we can calculate the normalized powers on the walls of the integrating sphere by using reflection and transmission values obtained with the adding–doubling method. The IAD algorithm calculates the normalized powers in the spheres and matches them to the detected powers (rather than matching reflection and transmission directly).

4. Accuracy of the Method

This section addresses the question: If R_T, T_T, and T_C are known exactly, what is the maximum possible error in the derived optical properties caused by the inverse adding–doubling method? The error analysis must be made numerically, because analytical expressions for light propagation in anisotropic media with mismatched boundaries are not available. The numerical tests are designed to find the accuracy of the inverse algorithm as functions of both the optical properties and the reflection and transmission of the sample. Implicit are checks on (a) the convergence of the inverse algorithm to the global minimum, (b) the termination criterion for stopping the iteration procedure, (c) the choice of starting parameters, and (d) the effect of using small numbers of quadrature points. This last test is particularly important, since the method would be useless (too slow) if small errors could be achieved only by using many quadrature points.

Generating a set of accurate testing values presented a problem, since accurate tabulated values for mismatched boundaries with anisotropic scattering could not be found in the literature. Consequently, after demonstrating that our adding–doubling implementation reproduced the published values for matched boundaries[24,46] exactly, we used Monte Carlo to verify a few mismatched cases. This confirmed the boundary condition algorithm. Finally, we compared 36- and 48-quadrature-point adding–doubling calculations. The 36-point calculation was always correct to at least 0.1%. The 48-point calculation was used for the test data and was constrained to include only samples with reduced optical thicknesses of > 0.25 and optical thicknesses of < 32. The rationale was that when $\tau' < 0.25$ either the sample does not multiply scatter and therefore a simpler algorithm should be used, or the sample does multiply scatter, but because of the highly anisotropic nature of each scattering event, the separation of T_C from

scattered light would be extremely difficult. The second criterion ($\tau < 32$) ensured that the sufficient collimated transmitted light passed through the sample so that it could be measured [$T_C > \exp(-32) \sim 10^{-14}$]. The IAD method works for any optical thickness, but it becomes progressively less accurate outside this range.

All samples assume slabs with an index of refraction of 1.4 relative to the environment. Results for the index-matched samples indicate that the error in the IAD method is approximately half of those presented here for the mismatched case. This is caused by total internal reflection of light at quadrature angles that are greater than the critical angle (one-half of the total number, see Subsection 2.C). The slabs are not sandwiched by glass: calculations with a sample between glass slides do not alter the mismatched ($n = 1.4$) results significantly and are omitted for brevity.

In all calculations the scattering phase function used was the Henyey–Greenstein phase function. Despite the limited experimental evidence that this phase function is appropriate for tissues, errors arising from an inappropriate phase function should be small, since different phase functions with equivalent g values and different higher-order moments generate nearly equal reflection and transmission values.[46]

The absolute error is defined as the difference between the true or accurate values and those calculated with the inverse adding–doubling method:

$$\Delta a' = |a_{\text{true}}' - a_{\text{calc}}'|. \tag{5}$$

The relative percentage error is the absolute error divided by the true value and multiplied by 100. The absolute errors in the scattering and absorption coefficients are proportional to the physical thickness of the sample and consequently are not particularly useful. The relative errors for μ_a and μ_s can also be obtained despite the fact that only dimensionless optical parameters are used by noting that the physical thickness cancels:

$$\frac{\Delta\mu_a}{\mu_a^{\text{true}}} = 100\left[1 - \frac{(1 - a_{\text{calc}})\tau_{\text{calc}}}{(1 - a_{\text{true}})\tau_{\text{true}}}\right],$$
$$\frac{\Delta\mu_s}{\mu_s^{\text{true}}} = 100\left(1 - \frac{a_{\text{calc}}\tau_{\text{calc}}}{a_{\text{true}}\tau_{\text{true}}}\right). \tag{6}$$

B. Variation with Optical Properties

The sensitivity of the inverse adding–doubling method to the optical properties of a sample was evaluated by using a data set consisting of reflection and transmission values for 11 reduced albedos spaced so that $(1 - a_{\text{true}}')^{1/2} = (0, 0.1, \ldots, 1)$, 10 anisotropies spaced similarly (0, 0.19, 0.36, 0.51, 0.64, 0.75, 0.84, 0.91, 0.96, 0.99), and 14 reduced optical depths (listed in Table 1). Thus for each pair (a', τ') there were 10 different values of g that all corresponded to more or less equal values of R_T, T_T. There was a total of 1540 different combinations of a_{true}, τ_{true}, g_{true}. For each combination accurate reflection and transmission (R_T, T_T, T_C) values were calculated. The optical properties were found by using the IAD method with four and eight quadrature points. Diffusion equation results were obtained by using the same iteration algorithm but by replacing the adding–doubling calculation with a δ-Eddington diffusion approximation.[22,48]

Table 1. Maximum Errors in the Calculated Reduced Optical Thickness τ' for any Albedo or Anisotropy as a Function of the True Reduced Optical Thickness[a]

	Maximum Absolute Errors			Maximum Relative Errors		
τ'	Diffusion	4	8	Diffusion	4	8
1/4	0.04	0.02	0.01	16	9	4
3/8	0.03	0.02	0.01	9	6	3
1/2	0.03	0.02	0.01	5	5	2
3/4	0.03	0.03	0.01	3	3	1
1	0.04	0.03	0.01	4	3	1
3/2	0.07	0.03	0.01	5	2	1
2	0.2	0.04	0.02	11	2	.8
3	0.2	0.04	0.02	7	1	.6
4	0.3	0.05	0.02	8	1	.6
6	0.6	0.1	0.04	10	1	.6
8	0.9	0.2	0.05	11	2	.6
12	1.5	0.3	0.09	12	2	.7
16	2	0.4	0.1	13	2	.7

[a]The calculated values were obtained by using a δ-Eddington approximation (diffusion) or the IAD method with four or eight quadrature points.

The spacing in the reduced albedo was based on the observation that reflection and transmission are quite sensitive to changes in the reduced albedo when it is near unity. The anisotropy was chosen to vary in a similar manner for the same reason. Completely forward scattering ($g = 1$) was omitted because it corresponds to the nonscattering case. The nonscattering ($a = 0$) and nonabsorbing ($a = 1$) cases were both included. The range of the reduced optical thickness was chosen because of the natural advantage of making calculations for optical thicknesses that vary by a factor of 2 when the adding–doubling technique is used.

The variation in IAD accuracy with reduced optical thickness is tabulated in Table 1 and displayed in Fig. 3. The maximum relative error for a fixed τ' is the greatest error in a calculated value of τ' for any albedo and scattering anisotropy. The relative error decreases as the number of quadrature points increases. When $1 \le \tau' \le 16$ the maximum relative error when four quadrature points are used is $< 2\%$. Surprisingly the diffusion approximation works best for $\tau' \approx 1$ but when only the relative error is considered. Table 1 shows that the maximum absolute error $\Delta\tau'$ monotonically increases with τ' for the diffusion approximation as well as the four- and eight-quadrature-point IAD calculations.

The variation in the relative error in the scattering

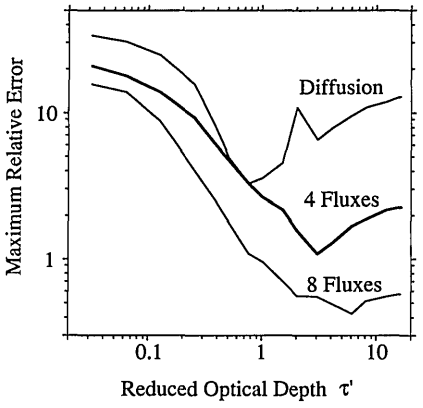

Fig. 3. Maximum error in the calculated reduced optical thickness τ' for any anisotropy and any albedo by using the diffusion approximation and the IAD method with four and eight quadrature points.

coefficient was evaluated for changes in the reduced optical thickness, the reduced albedo, and the scattering anisotropy when only four quadrature points were used. In Fig. 4 the maximum relative error in the calculated scattering coefficient is plotted as a function of the three dimensionless quantities a', τ', and g. As expected the accuracy in determining μ_s increases as the scattering increases (i.e., as $a' \rightarrow 1$). The increased scattering implies more uniform internal radiance distributions, which in turn are more accurately approximated than highly anisotropic internal radiance by four-quadrature-point distributions. Errors in the scattering coefficient do not depend strongly on either the reduced optical thickness or the scattering anisotropy. The maximum relative error never exceeds 6% for positive albedos.

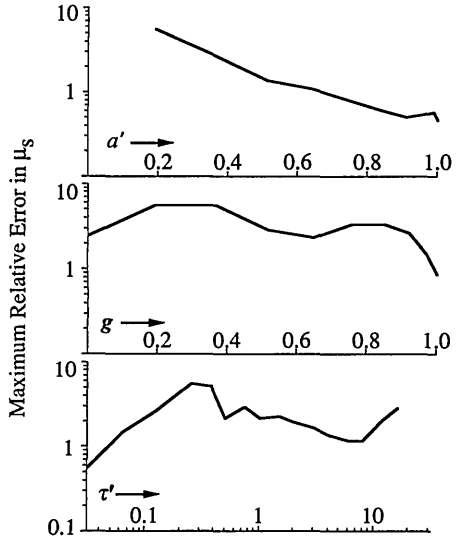

Fig. 4. Maximum relative error in the calculated scattering coefficient as a function of the reduced albedo a', the reduced optical thickness τ', and the scattering anisotropy g by using the IAD method with four quadrature points and mismatched boundaries $n = 1.4$.

B. Variation with Reflection and Transmission

The accuracy of the inverse adding–doubling method varies with the reflection and transmission of the sample. To quantify the maximum error for specific reflection and transmission values another paired set of a_{true}, τ_{true}, g_{true} and R_T, T_T, T_C were generated. In this set the total reflection and total transmission were spaced evenly (in 0.05 increments). By permitting the unscattered transmission to take on different values, 10 different sets of a_{true}, τ_{true}, g_{true} were obtained for each pair (R_T, T_T). The maximum relative error in the absorption coefficient, the scattering coefficient, and the scattering anisotropy was calculated by using the IAD method with four quadrature points.

Figure 5 shows a contour plot of the maximum relative error in the calculated absorption coefficient as a function of total reflection and total transmission. The maximum relative error in the absorption coefficient (assuming $\mu_a > 0$ or $R_T + T_T < 1$) was 10%. The $R_T + T_T = 0$ case is omitted because $\mu_a = 0$ for conservative scattering and the relative error is infinite in this case. For the majority of R_T, T_T combinations the maximum error is 2–3%. The error is greatest when the total transmission is highest, which corresponds to samples that absorb only a small fraction of the light.

Figure 6 shows a contour plot of the maximum relative error in the scattering coefficient as a function of the total reflection and total transmission. In contrast to the error in the absorption coefficient the error for the scattering coefficient is greatest when little light is reflected by the sample. The error drops sharply with increasing reflection values. The maximum error is always $<2\%$ for any nonzero value of μ_s. The $\mu_s = 0$ case is omitted for the same reason that conservative scattering is avoided in Fig. 5. The larger relative errors seen in Fig. 4 all correspond to the very small reflection values indicated by the black area in Fig. 6.

Figure 7 shows a contour plot of the maximum

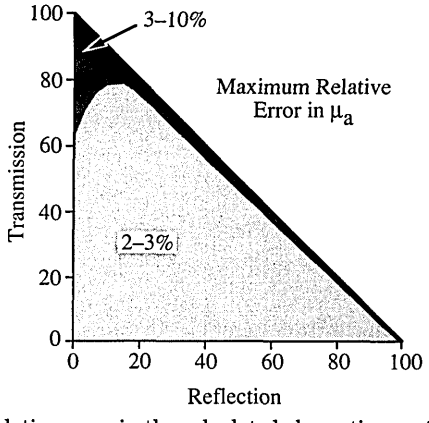

Fig. 5. Relative error in the calculated absorption coefficient as a function of reflection and transmission. The IAD method was used with four quadrature points, and the slab had mismatched boundaries.

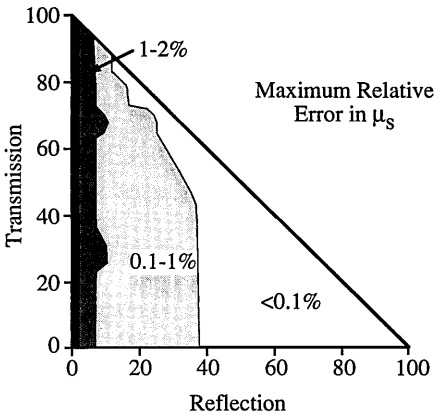

Fig. 6. Relative error in the calculated scattering coefficient as a function of reflection and transmission. The IAD method was used with four quadrature points, and the slab had mismatched boundaries.

absolute error in the scattering anisotropy as a function of total reflection and total transmission. The error is always < 0.03 for all the cases in which the scattering coefficient is nonzero. When the scattering coefficient is zero, no scattering takes place and any measurement will not give information on the shape of the scattering event. These cases correspond to total reflection values that are equal to the unscattered reflected light.

Typically the errors resulting from the IAD method will be much smaller than those resulting from experimental uncertainties. For example, assume that the measurements $R_T = 0.264$, $T_T = 0.261$, and $T_C = 5.91 \times 10^{-5}$ are known with a 1% uncertainty. The relative errors resulting from the IAD method are 0.04% for μ_s, 1% for μ_a, and 0.1% for g. However, perturbing the reflection and transmission values by 1% and re-solving for the optical properties result in errors of 0.4% for μ_s, 17% for μ_a, and 0.4% for g or approximately an order of magnitude larger than the errors inherent in the IAD method itself. Such error estimates are necessary because of the nonlinear relationship between reflection and transmission and the intrinsic optical properties. A primary goal of this study was to develop an accurate method of computing optical properties, so that such estimates can be made without introducing errors caused by the calculation itself.

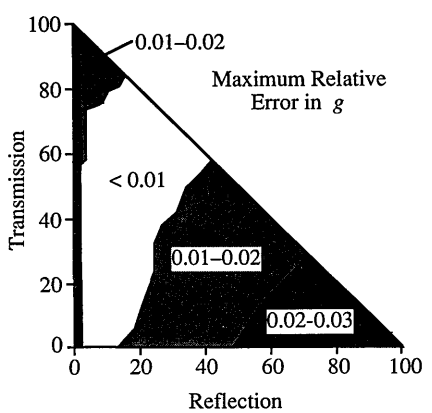

Fig. 7. Relative error in the calculated scattering anisotropy as a function of reflection and transmission. The IAD method was used with four quadrature points, and the slab had mismatched boundaries.

In practice the two most common sources of experimental errors are (1) loss of light from the edges of the sample (which thereby invalidates the one-dimensional assumptions and underestimating both R_T and T_T) and (2) collecting scattered light in the unscattered transmission measurement (which thereby overestimates T_C). The first problem manifests itself in spuriously high absorption values, and the latter case leads to optical properties that depend on the thickness of the sample. These problems are discussed at length in the experimental implementation of this technique.[1]

5. Conclusions

The inverse adding–doubling method translates total reflection, total transmission, and unscattered transmission measurements into scattering, absorption, and scattering anisotropy values. The method is applicable when the one-dimensional radiative transport equation adequately describes the propagation of light through the sample. Using only four quadrature points, the IAD method generates optical properties (μ_a, μ_s, g) that are accurate to 2–3% for most reflection and transmission values. Higher accuracy is achieved by using more quadrature points, but it requires increased computation time. The validity of the IAD method for samples in which ($\mu_a \approx \mu_s$) is especially important since other methods (e.g., those based on the diffusion approximation) are known to fail in this regime. Furthermore both anisotropic phase functions and Fresnel reflection at boundaries are accurately approximated, and therefore the IAD method is well suited to measurements involving biological tissues sandwiched between glass slides. A computer implementation of the inverse adding–doubling method is available from the authors.

This work was supported by the Office of Naval Research Contract N00014-86-K-0117 and the National Institutes of Health grant 5R01AR25395-11.

References

1. J. W. Pickering, S. A. Prahl, N. van Wieringen, J. B. Beek, H. J. C. M. Sterenborg, and M. J. C. van Gemert, "Double-integrating-sphere system for measuring optical properties of tissue," Appl. Opt. **32,** 399–410 (1993).
2. W. F. Cheong, S. A. Prahl, and A. J. Welch, "A review of the optical properties of biological tissues," IEEE J. Quantum Electron. **26,** 2166–2185 (1990).
3. M. S. Patterson, B. C. Wilson, and D. R. Wyman, "The propagation of optical radiation in tissue II. Optical properties of tissues and resulting fluence distributions," Lasers Med. Sci. **6,** 379–390 (1991).
4. B. C. Wilson, M. S. Patterson, and S. T. Flock, "Indirect versus

direct techniques for the measurement of the optical properties of tissues," Photochem. Photobiol. **46,** 601–608 (1987).
5. S. T. Flock, B. C. Wilson, and M. S. Patterson, "Total attenuation coefficients and scattering phase functions of tissues and phantom materials at 633 nm," Med. Phys. **14,** 835–841 (1987).
6. P. Kubelka, "New contributions to the optics of intensely light-scattering materials. Part I," J. Opt. Am. **38,** 448–457 (1948).
7. P. Kubelka, "Errata: new contributions to the optics of intensely light-scattering materials," J. Opt. Soc. Am. **38,** 1067 (1948).
8. P. Kubelka, "New contributions to the optics of intensely light-scattering materials. Part II: Nonhomogeneous layers," J. Opt. Soc. Am. **44,** 330–335 (1954).
9. J. T. Atkins, "Optical properties of turbid materials," in *The Biologic Effects of Ultraviolet Radiation (With Emphasis on the Skin)*, F. Urbach, ed. (Pergamon, London, 1969), pp. 141–149.
10. S. Q. Duntley, "The optical properties of diffusing materials," J. Opt. Soc. Am. **32,** 61–70 (1942).
11. A. L. Lathrop, "Diffuse scattered radiation theories of Duntley and of Kubelka–Munk," J. Opt. Soc. Am. **55,** 1097–1104 (1965).
12. B. L. Diffey, "A mathematical model for ultraviolet optics in skin," Phys. Med. Biol. **28,** 647–657 (1983).
13. G. M. LaMuraglia, M. R. Prince, N. S. Nishioka, S. Obremski, and R. Birngruber, "Optical properties of human arterial thrombus, vascular grafts, and sutures: implications for selective laser thrombus ablation," IEEE J. Quantum Electron. **26,** 2200–2206 (1990).
14. A. Vogel, C. Dlugos, R. Nuffer, and R. Birngruber, "Optical properties of human sclera, and their consequences for transscleral laser applications," Lasers Surg. Med. **11,** 331–340 (1991).
15. P. S. Mudgett and L. W. Richards, "Multiple scattering calculations for technology," Appl. Opt. **10,** 1485–1502 (1971).
16. J. Reichman, "Determination of absorption and scattering coefficients for nonhomogeneous media. 1: Theory," Appl. Opt. **12,** 1811–1815 (1973).
17. W. G. Egan, T. W. Hilgeman, and J. Reichman, "Determination of absorption and scattering coefficients for nonhomogeneous media. 2: Experiment," Appl. Opt. **12,** 1816–1823 (1973).
18. S. A. Prahl, I. A. Vitkin, B. C. Wilson, and R. R. Anderson, "Determination of optical properties of turbid media using pulsed photothermal radiometry," Phys. Med. Biol. **37,** 1203–1217 (1992).
19. M. S. Patterson, B. Chance, and B. C. Wilson, "Time resolved reflectance and transmittance for the noninvasive measurement of tissue optical properties," Appl. Opt. **28,** 2331–2336 (1989).
20. M. S. Patterson, E. Schwartz, and B. C. Wilson, "Quantitative reflectance spectrophotometry for the noninvasive measurement of photosensitizer concentration in tissue during photodynamic therapy," in *Photodynamic Therapy: Mechanisms,* T. J. Dougherty, ed., Proc. Soc. Photo-Opt. Instrum. Eng. **1065,** 115–122 (1989).
21. K. M. Yoo, F. Liu, and R. R. Alfano, "Angle and time resolved studies of backscattering of light from biological tissues," in *Laser–Tissue Interaction,* S. L. Jacques, ed., Proc. Soc. Photo-Opt. Instrum. Eng. **1202,** 260–271 (1990).
22. S. L. Jacques and S. A. Prahl, "Modeling optical and thermal distributions in tissue during laser irradiation," Lasers Surg. Med. **6,** 494–503 (1987).
23. G. Yoon, S. A. Prahl, and A. J. Welch, "Accuracies of the diffusion approximation and its similarity relations for laser irradiated biological media," Appl. Opt. **28,** 2250–2255 (1989).
24. H. C. van de Hulst, *Multiple Light Scattering* (Academic, New York, 1980), Vol. 1.
25. G. N. Plass, G. W. Kattawar, and F. E. Catchings, "Matrix operator theory of radiative transfer. 1: Rayleigh scattering," Appl. Opt. **12,** 314–329 (1973).
26. S. Chandrasekhar, *Radiative Transfer* (Dover, New York, 1960), Chap. 8.
27. S. E. Orchard, "Reflection and transmission of light by diffusing suspensions," J. Opt. Soc. Am. **59,** 1584–1597 (1969).
28. B. C. Wilson and G. Adam, "A Monte Carlo model for the absorption and flux distributions of light in tissue," Med. Phys. **10,** 824–830 (1983).
29. S. A. Prahl, M. Keijzer, S. L. Jacques, and A. J. Welch, "A Monte Carlo model of light propagation in tissue," in *Dosimetry of Laser Radiation in Medicine and Biology,* G. J. Müller and D. H. Sliney, eds., Proc. Soc. Photo-Opt. Instrum. Eng. **ISO 5,** 102–111 (1989).
30. S. T. Flock, M. S. Patterson, B. C. Wilson, and D. R. Wyman, "Monte Carlo modeling of light propagation in high scattering tissue—I: Model predictions and comparison with diffusion theory," IEEE Trans. Biomed. Eng. **BME-36,** 1162–1168 (1989).
31. R. Bellman and G. M. Wing, *An Introduction to Invariant Imbedding* (Wiley, New York, 1975).
32. J. W. Pickering, C. J. M. Moes, H. J. C. M. Sterenborg, S. A. Prahl, and M. J. C. van Gemert, "Two integrating spheres with an intervening scattering sample," J. Opt. Soc. Am. A **9,** 621–631 (1992).
33. S. L. Jacques, C. A. Alter, and S. A. Prahl, "Angular dependence of HeNe laser light scattering by human dermis," Lasers Life Sci. **1,** 309–333 (1987).
34. G. Yoon, A. J. Welch, M. Motamedi, and M. C. J. V. Gemert, "Development and application of three-dimensional light distribution model for laser irradiated tissue," IEEE J. Quantum Electron. **QE-23,** 1721–1733 (1987).
35. H. C. van de Hulst, *A New Look at Multiple Scattering,* Tech. Rep. (NASA Institute for Space Studies, New York, 1962).
36. W. M. Irvine, "Multiple scattering in planetary atmospheres," Icarus **25,** 175–204 (1975).
37. R. Priesendorfer, *Hydrologic Optics* (U.S. Department of Commerce, Washington, D.C., 1976), Vol. 1.
38. W. J. Wiscombe, "On initialization, error and flux conservation in the doubling method," J. Quant. Spectrosc. Radiative Transfer **16,** 637–658 (1976).
39. W. J. Wiscombe, "Doubling initialization revisited," J. Quant. Spectrosc. Radiat. Transfer **18,** 245–248 (1977).
40. W. J. Wiscombe, "The delta-M method: rapid yet accurate radiative flux calculations for strongly asymmetric phase functions," J. Atmos. Sci. **34,** 1408–1422 (1977).
41. K. M. Case and P. F. Zweifel, *Linear Transport Theory* (Addison-Wesley, Reading, Mass., 1967), Chap. 8, p. 226.
42. W. H. Press, B. P. Flannery, S. A. Teukolsky, and W. T. Vetterling, *Numerical Recipes: The Art of Scientific Computing* (Cambridge U. Press, New York, 1986), Chap. 10, p. 289.
43. F. B. Hildebrand, *Introduction to Numerical Analysis* (Dover, New York, 1974), Chap. 8.
44. F. P. Bolin, L. E. Preuss, R. C. Taylor, and R. J. Ference, "Refractive index of some mammalian tissues using a fiber optic cladding method," Appl. Opt. **28,** 2297–2303 (1989).
45. J. A. Nelder and R. Mead, Comput. J. **7,** 380 (1965).
46. H. C. van de Hulst, *Multiple Light Scattering* (Academic, New York, 1980), Vol. 2. Chap. 14.
47. M. J. C. van Gemert and W. M. Star, "Relations between the Kubelka–Munk and the transport equation models for anisotropic scattering," Lasers Life Sci. **1,** 287–298 (1987).
48. J. H. Joseph, W. J. Wiscombe, and J. A. Weinman, "The delta-Eddington approximation for radiative flux transfer," J. Atmos. Sci. **33,** 2452–2459 (1976).